

## Article

# Oxidation of Alcohols into Carbonyl Compounds Using a CuO@GO Nano Catalyst in Oxygen Atmospheres

Maqsood Ahmad Malik <sup>1,\*</sup> , Ravikumar Surepally <sup>2</sup>, Nagarjuna Akula <sup>3</sup>, Ravi Kumar Cheedarala <sup>3,4,\*</sup>, Abdulmohsen Ali Alshehri <sup>1</sup>  and Khalid Ahmed Alzahrani <sup>1</sup>

<sup>1</sup> Chemistry Department, Faculty of Sciences, King Abdulaziz University, P.O. Box 80203, Jeddah 21589, Saudi Arabia

<sup>2</sup> Research & Development, Ajmal Perfumes Manufacturing & Oudh Processing Industry (L.L.C.), Dubai P.O. Box 3141, United Arab Emirates

<sup>3</sup> Department of Chemistry, JNTU College of Engineering, Kukatpally, Hyderabad 500050, Telangana, India

<sup>4</sup> School of Mechanical Engineering, Changwon National University, Changwon 51139, Republic of Korea

\* Correspondence: mamalik@kau.edu.sa (M.A.M.); rkchidrala@gmail.com (R.K.C.)

**Abstract:** In this article, the oxidation of alcohols into carbonyl compounds was studied in oxygen atmospheres using a copper oxide on graphene oxide (CuO@GO) nano composites catalyst, synthesized by the wet chemistry method. CuO@GO nano composites were prepared from GO, and CuO NPs by the sol-gel method. The transformation of aromatic alcohols into corresponding carbonyl compounds in good-to-high yields were observed using the CuO@GO catalyst under an oxygen atmosphere. Synthesized CuO@GO was confirmed by FT-IR, XRD, XPS, TEM, FE-SEM, TEM, and SEM analyses, and revealed intercalation of CuO-NPs on/in GO nano sheets through the chelation of Cu<sup>+2</sup> ions with CO, COOH, and OH groups presenting on the GO nano sheets. The catalytic activity of CuO@GO nano composites for the conversion of alcohols into carbonyl compounds were evaluated through TOF ( $2.56 \times 10^{-3} \text{ mol g}^{-1} \text{ min}^{-1}$ ). The use of CuO@GO has shown catalytic activity and recyclability with a high conversion of alcohols to ketones. We assume that the proposed CuO@GO catalyst can be used for other key organic transformations and will be evaluated in the future.

**Keywords:** catalysis; CuO@GO; TOF; alcohols; ketones; oxidation; GO



**Citation:** Malik, M.A.; Surepally, R.; Akula, N.; Cheedarala, R.K.; Alshehri, A.A.; Alzahrani, K.A. Oxidation of Alcohols into Carbonyl Compounds Using a CuO@GO Nano Catalyst in Oxygen Atmospheres. *Catalysts* **2023**, *13*, 55. <https://doi.org/10.3390/catal13010055>

Academic Editor: Victorio Cadierno

Received: 8 October 2022

Revised: 18 December 2022

Accepted: 21 December 2022

Published: 27 December 2022



**Copyright:** © 2022 by the authors. Licensee MDPI, Basel, Switzerland. This article is an open access article distributed under the terms and conditions of the Creative Commons Attribution (CC BY) license (<https://creativecommons.org/licenses/by/4.0/>).

## 1. Introduction

The oxidation of aromatic alcohols into carbonyl compounds is a ubiquitous transformation in nature. Numerous oxidizing agents such as palladium [1], platinum [2–4], chromium (VI) reagents [5], and manganese [6] or ruthenium [7] salts have attracted much attention to promote this key transformation. In many cases, these reagents are required in stoichiometric amounts and are normally toxic, hazardous, or both. Recently, Wang et al. reported bi-metallic catalysis composed of CuO with gold and platinum for the catalytic oxidation of alcohols, because CuO alone cannot catalyze the oxidation reaction since the adsorption of alcohols onto the CuO surface was too weak and could not activate the O<sub>2</sub> molecule [8]. Due to this reason, they examined the catalytic activity of a bimetallic catalyst composed of gold nanoparticles supported on copper oxide for oxidation of alcohols. In another report, Poreddy et al. investigated the highly selective oxidative dehydrogenation of benzylic, alicyclic, and unsaturated alcohols using CuO nanoparticles in an N-cyclohexyl-3-aminopropane sulfonic acid buffer solution under air conditions [9]. They suggested a possible reaction mechanism for oxidative dehydrogenation was involved, through a β-H elimination step. However, for oxidation reactions, one or more equivalents of such relatively expensive oxidizing agents are an important factor in limiting their usage in the industry today. In addition, problems relating to decay and plating on reactor walls, and handling, recovery, and reuse of the catalyst represent serious process limitations [10]. Therefore, it is very urgent to replace stoichiometric oxidants with alternative, cheaper,

more sustainable catalysts, and methodologies required to mimic nature have gained much interest. Our interest is in the selective oxidation of alcohols into carbonyl compounds using non-noble metal catalysts. Thus, copper oxide nanoparticles have gained much attention in recent years because of their advantages as being less toxic and cheaper for the oxidation of alcohols under mild reaction conditions.

CuO is widely used as the cheapest metal oxide in the field of catalysis [11], superconducting materials [12], gas sensors [13], photoconductive and photothermal applications [14], semiconductors [15], solar energy transformation [16], thermoelectric materials [17], and as rocket-propellant combustion catalysts [18]. With the outstanding catalytic property of CuO as a catalyst in various fields, we attracted to design a new catalytic system that is composed of CuO-NPs embedded in graphene oxide (GO) nanolayers [19].

Here, we report a highly efficient, aerobic catalytic reaction system in O<sub>2</sub> atmosphere for the conversion of alcohols into carbonyl compounds. In situ generation of CuO nanoparticles and intercalated with GO layers to produce a novel heterogeneous catalyst as a CuO@GO. In the literature, the CuO nanoparticles were used for the oxidation of alcohols into carbonyl compounds, but it provided poorer yields. To reach fast reaction times, higher yields, catalyst recyclability, and to stop generation of toxic wastes, we developed an alternative robust nanocatalytic system such as CuO@GO [20]. Furthermore, CuO@GO is a highly stable and reusable catalyst. CuO nanoparticles have proved to be an attractive catalyst in many useful organic transformations including oxidations, cyclization, C-N bond formation, etc. [21–23]. The present work was inspired by our previous research reports on the aerobic oxidation of alcohols mediated by Pd/AIOOH heterogeneous catalyst [24,25], as shown in Figure 1.



Figure 1. Synthesis of GO, CuO@GO, and oxidation of alcohols into carbonyls (Stages 1, 2 & 3).

## 2. Results and Discussion

### 2.1. FT-IR Spectroscopy

The FT-IR spectrum of GO and CuO@GO is in good agreement with reported literature, as shown in Figure 2a. In particular, the characteristic peaks of GO at 3424 cm<sup>-1</sup> for hy-

droxyl (-OH),  $2890\text{ cm}^{-1}$  for methylene ( $\text{CH}_2$ ),  $1741\text{ cm}^{-1}$ , and  $1564\text{ cm}^{-1}$  for carbonyls (CO, and COOH),  $1211\text{ cm}^{-1}$  for alkoxy (-COC-), and  $1072\text{ cm}^{-1}$  for -CH groups [26,27]. Next, the  $\text{Cu}(\text{OAc})_2 \cdot \text{H}_2\text{O}$  was reduced into CuO NPs, and simultaneously coordinated with the -CO- and -COOH groups of GO nanolayers. The vibrational bands of CuO@GO at  $3450\text{ cm}^{-1}$  and  $3350\text{ cm}^{-1}$  corresponded to the hydroxyl (-OH) of COOH and Cu-OH [28,29]. The stretching bands were at  $2892\text{ cm}^{-1}$  for the methylene ( $\text{CH}_2$ ) group,  $1732\text{ cm}^{-1}$  and  $1626\text{ cm}^{-1}$  for carbonyl (-CO-) from GO,  $1573\text{ cm}^{-1}$  from the Cu-O stretching band,  $1424\text{ cm}^{-1}$  for -CH,  $1342\text{ cm}^{-1}$  for Cu-O bending,  $1212\text{ cm}^{-1}$  for COC,  $1076\text{ cm}^{-1}$  for -CH-bending, and at  $635\text{ cm}^{-1}$  for Cu-O bending peaks [30]. All the new peaks in CuO@GO moved  $\sim 2$  to 3 units, due to the formation of coordination Cu(II) ions with GO nanolayers. These results suggested that the CuO was strongly exfoliated within GO nanolayers.

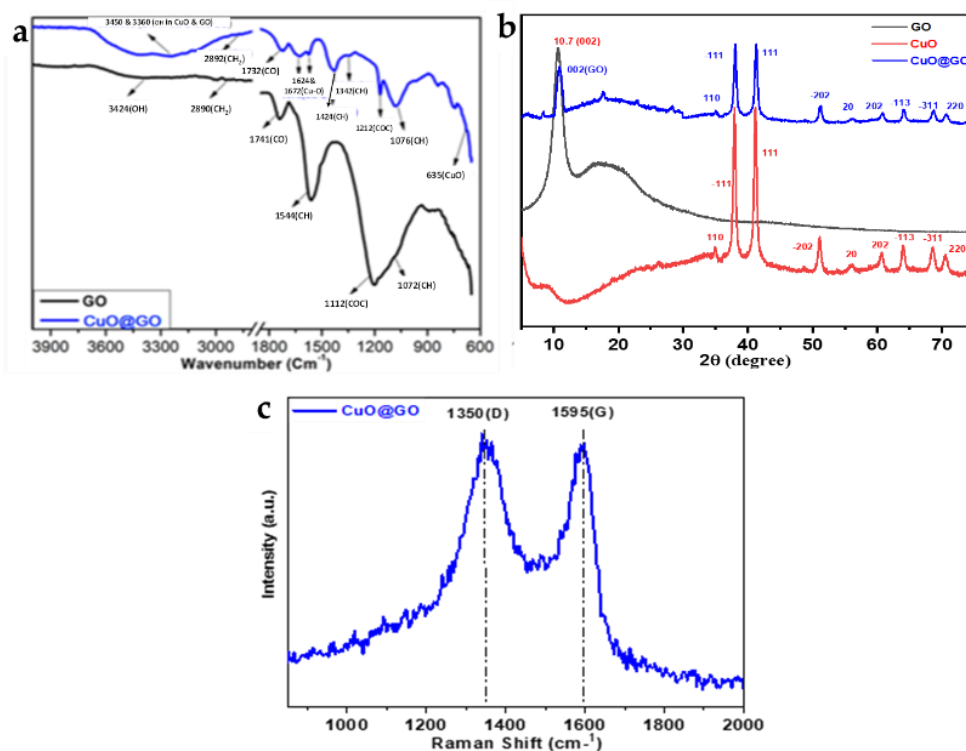


**Figure 2.** (a) FT-IR spectra for GO and CuO@GO; (b) XRD spectra for GO, CuO, and CuO@GO; (c) Raman spectra of CuO@GO.

## 2.2. XRD Spectroscopy

The typical XRD patterns of CuO-NPs, GO, and CuO@GO are depicted in Figure 2b. The XRD pattern of GO is amorphous, CuO nanoparticles are found as crystalline, whereas as-synthesized CuO@GO nanocomposites were semi-crystalline in nature. The XRD spectrum was indistinguishable from that of pure CuO, representing the establishment of single-phase CuO nanoparticles by a monoclinic structure (JCPDS-05-0661) [31]. In the present work, the  $2\theta$  values of 35.7 (110), 38.9 (-111), 42.1 (111), 52.9 (-202), 56.9 (020), 61.7 (202), 65.5 (-113), 69.4 (-311), and 71.5 (220) were allocated to the reflection lines of monoclinic CuO-NPs. The results have been established to agree with the reported diffraction pattern of CuO NPs prepared by Zang et al. [30]. It can be seen that there were two distinct diffraction peaks that appeared as a broad hump and sharp peak at  $2\theta$  values of 10.78 belonging to the (002) plane of GO, and interlayer spacing was much larger than that of GO layers due to the introduction of CuO within the GO sheets. Next, the XRD pattern of CuO@GO showed a similar pattern to in a water isopropanol system, and the  $2\theta$  values were observed at 10.75 (002), 36. those of the CuO-NPs monoclinic phase (PCPDS 80-1268) [32,33]. The reflection peak at 10.7  $2\theta$  (002) indicated that GO exfoliated strongly within the GO sheets, owing to the invasion of CuO NPs [31,32]. The peaks pattern demon-

strated that CuO@GO can be successfully achieved 16 (110), 39.19 (-111), 42.42 (111), 52.3 (-202), 57.88 (020), 61.6 (202), 64.8 (-113), 69.44 (-311), and 71.3 (220). The peaks were moved from 0.2 to 0.28 units, and the representative signal of GO at 10.78 (002) disappeared and transformed into a broad hump with minor reflection peaks. Furthermore, the composition of the CuO@GO nanocomposite catalyst was further described by Raman spectroscopy to verify the GO support, as shown in Figure 2c. The G line (first-order scattering of the E<sub>2g</sub> phonons of sp<sup>2</sup> orbital) at 1595 cm<sup>-1</sup>, and D line (k-point phonons of A<sub>1g</sub> symmetry) at 1350 cm<sup>-1</sup> are clearly acquired for the CuO@GO nanocomposite catalyst as specific characteristics of GO [33]. The obtained CuO@GO nano catalyst is showed superior catalytic activity due to the presence of CuO nanoparticles anchored within GO layers for enhancing the catalytic activity of oxidation of alcohols to ketones in high yields.

### 2.3. XPS Analysis

Figure 3 showed the XPS spectra of GO, CuO-NPs, and CuO@GO. As can be realized from the spectra, the XPS survey scans of clean GO showed binding energies that showed the characteristic peaks of carbon and oxygen only. The observed C1s peaks assigned to C-C (284.75 eV), C-O (286.28 eV), and C=O (288.52 eV) functional groups presented in GO agree with the literature, see Figure 3a [34]. The C-O and C=O peaks were associated with hydroxyl and carboxylate groups which were presented in the GO. The C=O group may be seen due to the carbonyl and carboxylate groups present in the GO. The Cu 2p core-level spectrum in Figure 3b represents two strong peaks which were located at 933.4 and 954.2 eV, conforming to the Cu 2p<sup>3/2</sup> and Cu 2p<sup>1/2</sup>, respectively. These values were well matched with the data described for the Cu(2p) in CuO [35]. Figure 3c demonstrates that the Cu 2p<sup>3/2</sup> spectrum showed that the Cu<sup>2+</sup> peak lies at 932.4 eV, through two shake-up satellites 7.2 and 9.8 eV higher in binding energy than that of the main peak [36]. The major XPS peaks of CuO@GO appeared at 954.3 eV for Cu 2p<sup>3/2</sup> and 933.4 eV for Cu 2p<sup>1/2</sup>, along with minor peaks at 959.02 eV and at 940.7 eV for Cu<sub>2</sub>O, respectively. In addition, there were still minor energy peaks found at 963 eV and at 944.18 eV, which correspond to traces of Cu(OH)<sub>2</sub> within the matrix. The surface property of CuO/CuO-GO nanoparticles was studied by XPS analysis. The Cu 2p<sup>3/2</sup> core level was employed to investigate Cu surface oxidation. Figure 3d shows the main and the satellite peaks of Cu 2p<sup>3/2</sup> and Cu 2p<sup>1/2</sup> of the samples. These spectra are normalized based on the intensity of the main peak of Cu 2p<sup>3/2</sup>. Copper oxide can exist in two semiconducting phases, namely cupric oxide (CuO) and cuprous oxide (Cu<sub>2</sub>O). The broad Cu 2p<sup>3/2</sup> peak has been deconvoluted into two peaks, which are marked as Cu<sub>2</sub>O or Cu and CuO, respectively. Cu and Cu<sub>2</sub>O cannot be resolved by this deconvolution. because their binding energies are very close and are different by only 0.1–0.4 eV. Therefore, Cu(I) existed in the XPS spectra. Next, the C1s binding energy peaks were assigned to the C-C (284.8 eV), C-O (286.5 eV), and C=O (288.6 eV) functional groups presented in GO. The XPS results justified that the CuO@GO were strongly composed of CuO and GO. The strong shake-up satellites recorded in the CuO sample confirmed that Cu metal showed a Cu<sup>+2</sup> oxidation state and ruled out the possibility of the existence of a Cu<sub>2</sub>O phase [37]. In addition, a relatively narrow boning peak at 531.98 eV represented the presence of O1S<sup>1/2</sup> transition in CuO@GO. This transition appeared to arise mainly the CuO phase is probably shown in three kinds of oxygen constituents, namely O-Cu, HO-Cu, and surface oxygen (O-surface), with binding energies of 529.1, 530.6, and 531.5 eV, correspondingly [36].

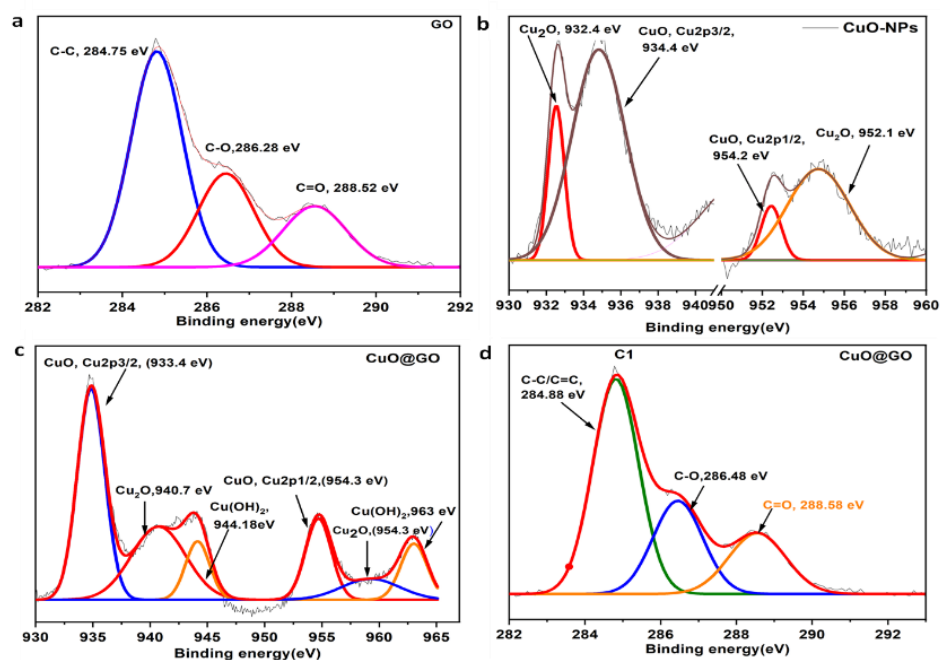


**Figure 3.** C1s spectra of GO (a); CuO (b) and CuO@GO (c,d).

#### 2.4. TEM, and SEM Analyses

TEM and SEM analyses were used to assess the surface morphology, actual size, and shape of GO, CuO-NPs, and CuO@GO, respectively, as shown in Figure 4. Mainly, Figure 4a shows few-layered GO nanosheets with smooth surfaces and wrinkles. The CuO-NPs were anchored on/in GO nanosheets through a chelation process by coordinate covalent bonds. Next, the CuO NPs were consistently deposited on the GO nanosheets with a strong binding effect of oxygen-containing groups, as shown in Figure 4b [38]. In addition, the inset image strongly supports the spherical-shaped CuO NPs on GO (CuONPs@GO), Figure 4c.

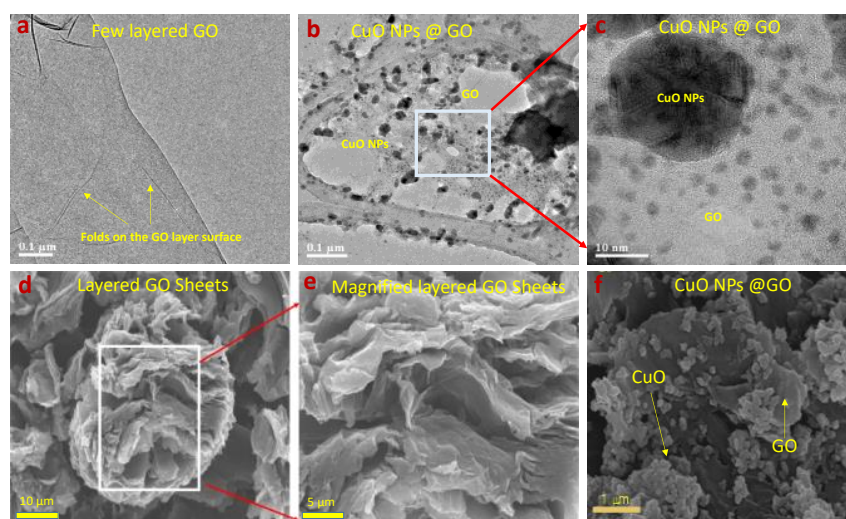


**Figure 4.** TEM and SEM micrographs of CuO-NPs on GO (a) few-layered GO sheets (0.1  $\mu\text{m}$ ); (b) CuO@GO (0.1  $\mu\text{m}$ ); (c) inset image of CuO on GO (10 nm); (d) pure-layered GO sheets (10  $\mu\text{m}$ ); (e) magnified layered GO sheets (5  $\mu\text{m}$ ); (f) dense CuO@GO (1  $\mu\text{m}$ ).

As shown in Figure 4d,e, the FE-SEM analyses confirms the successful formation of the CuO@GO nanocomposites. The results are on par with earlier publications in similar fields [30]. The surface morphologies of the CuO@GO sheets have crumpled

paper-like GO sheets, with few-to-several layers and air gaps, as shown in Figure 4d,e. In addition, CuO NPs were strongly anchored through C=O, COOH, and OH functional groups of GO nanosheets. In CuO@GO, particles of CuO with uniform size are selectively grown and uniformly distributed on the GO sheets, as shown in Figure 4f. In addition, an agglomeration of CuO nanoparticles with ionic clusters was found on the surface of GO nanosheets due to ionic linkages between CuO NPs. Furthermore, the uniform distribution and strong attachment of CuO nanoparticles on single or few-layered GO sheets can enhance the catalytic activity and reusability of CuO@GO without leaching of CuO while oxidating alcohols [39].

### 2.5. Screening of CuO@GO for the Oxidation of *p*-Methyl Benzyl Alcohol to *p*-Methyl Benzaldehyde

The optimized reaction conditions were established for the formation of carbonyl compounds from alcohols using CuO@GO by varying catalyst mole ratios at different periods and temperatures. Thus, the ideal reaction conditions are 1.0 mmol of alcohol and 0.2 g of CuO@GO under oxygen conditions at 80 °C in toluene for 6 h. The efficacy of CuO@GO for the oxidation of *p*-methyl benzyl alcohol to *p*-methyl benzaldehyde was examined in comparison with different mole ratios of CuO@GO catalyst (Table 1). Here, in the primary experiment, we made an attempt at an oxidation reaction using GO as a catalyst in toluene with O<sub>2</sub> atmosphere, no product yields were found after 10 h, and we recovered starting materials (entry 1). Next, we studied similar oxidation reaction conditions using 5 mol % of CuO-NPs and showed 78% yield for 6 h in O<sub>2</sub> (entry 2). It is worth mentioning that the oxidation process was gradually accelerated while increasing the mol % of CuO@GO from 0.5 to 2.0 in high yields (entries 3–5). The highest conversion of *p*-methyl benzyl alcohol to *p*-methyl benzaldehyde was found using 2 mol % of CuO@GO (entry 6), and no higher oxidation conversion occurred, even after 3 mol % of catalyst used (entry 7). Next, PdO/CuO-Y, MES-CuO, and Com-CuO showed poorer yields compared to the CuO@GO with 3 mol % and prolonged reaction times (entries 8 to 10), respectively. Next, the CuO@GO catalytic activity was demonstrated and obtained best results, as indicated by the high TOF ( $2.56 \times 10^{-3} \text{ mol g}^{-1} \text{ min}^{-1}$ ). This result is in agreement with our working hypothesis that most surfaces of these attached CuO NPs on GO nanosheets are exposed to the reaction environment. Hence, higher catalytic activity was observed with the CuO@GO nano sheets catalyst. These results show that this method is superior to the other methods in terms of yield and reaction time. In conclusion, CuO@GO with 2 mol % has shown the highest conversion ability for the oxidation reaction due to strong depositions of CuO on the GO nanosheets.

**Table 1.** Catalytic oxidation of *p*-methyl benzyl alcohol into *p*-methyl benzaldehyde under various conditions <sup>[a]</sup>.

Entry	Catalyst	CuO mol %	Reaction Time [h]	Conversion [%] <sup>[b]</sup>	Yield [%] <sup>[c]</sup>	TOF ( $\times 10^{-3} \text{ mol.g}^{-1}.\text{min}^{-1}$ ) <sup>[f]</sup>
1	GO	5	4(10)	<00	00	0.0
2	CuO-NPs	5	4(6)	75(78)	66	0.7
3	CuO@GO	0.5	4(6)	78(83)	69	1.16
4	CuO@GO	1.0	4(6)	84(87)	73	1.54
5	CuO@GO	1.5	4(6)	93(95)	85	1.93
6	CuO@GO	2.0	4(6)	98(98)	96(97)	2.56
7	CuO@GO	3.0	4(6)	98(99)	96(97)	2.59
8	PdO/CuO-Y	2.0	1	70	70 <sup>[d]</sup>	1.22
9	MES-CuO	3.0	24	71	71 <sup>[e]</sup>	1.22
10	Com-CuO	3.0	24	69	68 <sup>[e]</sup>	1.15

<sup>[a]</sup> Reaction conditions: A solution of *p*-methyl benzyl alcohol (1.0 mmol) in toluene (10 mL) was heated in the presence of catalyst 2 mol % of CuO@GO at 80 °C, 1 atm of O<sub>2</sub> for 6 h. <sup>[b]</sup> Determined by GC and <sup>1</sup>HNMR using TMS an internal standard. <sup>[c]</sup> Isolated yields. <sup>[d]</sup> Value in the parentheses is reaction times at 6 h and their corresponding yields. <sup>[d, e, f]</sup> References [40–42].

Figure 5 shows the CuO@GO catalyst's selectivity and recyclability. In addition, it can be recovered by filtration or decantation methods to save the catalyst (Table 2). To the best of our knowledge, CuO@GO is the first recyclable catalyst for the oxidation of various alcohols into corresponding carbonyl compounds in toluene at 80 °C for 6 h. Until the fourth cycle, the catalytic activity remains active, owing to the strong dispersion of the CuO@GO in toluene solvent as shown in Figure 5a. The proposed CuO@GO catalytic system has been improved quantitatively by a simple percolation, and recycled with reliable actions even after the fourth cycle. These results were attractive for the oxidation of alcohols into corresponding carbonyl compounds using CuO@GO. After the completion of the oxidation reaction, the leaching of CuO@GO was tested by ICP-AES. A moderate decrease in the catalytic efficacy of recovered CuO@GO may be due to the loss of catalysts during centrifugation and handling. However, after the fourth recycle, the catalyst activity gradually decreased due to the leaching of CuO in  $\mu\text{g}/\text{mL}$  of CuO@GO nanosheets, which can reduce the dispersibility within toluene, as shown in Figure 5b [43].

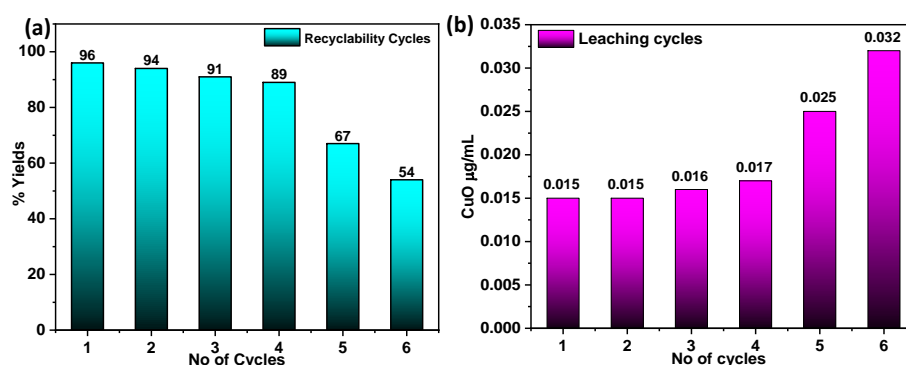


Figure 5. (a) Recycling and (b) leaching process of CuO@GO during oxidation process.

Table 2. Recycling of CuO@GO for the oxidation of p-methylbenzyl alcohol [a].

Use	T [°C]	T [h]	Yield [b, c]	Leaching of CuO $\mu\text{g}/\text{mL}$
1	80	6	96	0.015
2	80	6	94	0.015
3	80	6	91	0.016
4	80	6	89	0.017
5	80	6	67	0.025
6	80	6	54	0.032

[a] A solution of p-methyl benzyl alcohol (1.0 mmol), in toluene (5 mL) was heated at 80 °C in the presence of CuO@GO under 1 atm of O<sub>2</sub> for 10 h. [b] Determined by GC. [c] Isolated yields.

Table 3 shows the oxidation methodology of various alcohols such as aryl, substituted aromatic, cyclic aliphatic, and hetero aromatic alcohols to produce the corresponding carbonyl compounds in good to excellent yields. P-methyl benzyl alcohol was oxidized to obtain corresponding p-methyl benzaldehydes with a 93% yield in 4h (entry 1). Careful examination of the oxidation process revealed that the presence of electron-rich and electron-deficient groups does not show a significant effect on the aromatic ring; the oxidation reactions of benzyl alcohol (94%) were similar to those of 4-hydroxy benzyl alcohol (92%), and 4-nitrobenzyl alcohol (94%) (entries 2, 3 and 4) and anthracene-9-methanol to the corresponding aldehyde; i.e., anthracene-9-carbaldehyde in 95% yield (entry 5) and cyclopentanone were yielded at 88% after the smooth oxidation of cyclopentanone (entry 6).

**Table 3.** Catalytic oxidation of various alcohols into carbonyl compounds using CuO@GO [a].

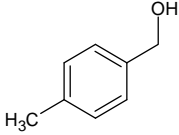
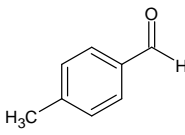
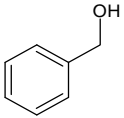
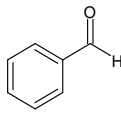
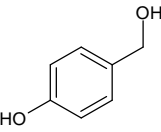
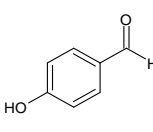
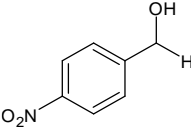
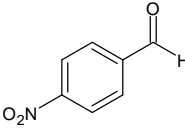
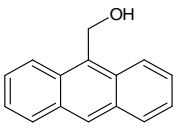
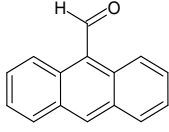
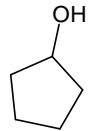
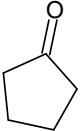
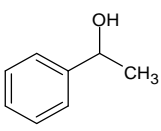
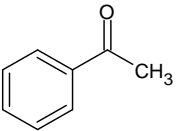
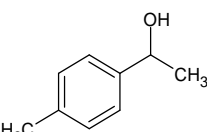
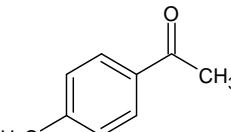
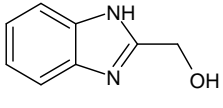
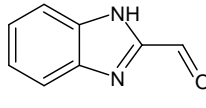
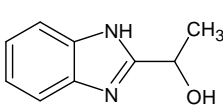
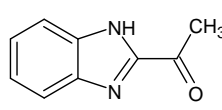
Entry	Substrate	Reaction Time	Product	Yield [b, c] (%)	<sup>1</sup> H NMR (300 MHz, CDCl <sub>3</sub> , δ ppm)
1		4		93(98) [d]	4-Methylbenzaldehyde (entry 1): 10.01 (s, 1H, CHO), 7.73 (d, 2H, aryl), 7.24 (d, 2H, aryl), 2.45 (s, 3H, CH <sub>3</sub> ).
2		4		94(99) [d]	Benzaldehyde (entry 2): 9.91 (s, 1H, CHO), 7.7–7.51 (m, 5H, aryl).
3		5		92(98) [d]	4-Hydroxybenzaldehyde (entry 3): 9.86 (s, 1H, CHO), 7.82 (d, 2H, aryl), 6.98 (d, 2H, aryl), 6.52 (brs, 1H, OH).
4		6		94(98) [d]	4-Nitrobenzaldehyde (entry 4): 10.17 (s, 1H, CHO), 8.35 (d, 2H, aryl), 8.10 (d, 2H, aryl).
5		6.5		95	(entry 5), 9-Anthraldehyde (entry 5): 10.9 (s, 1H, CHO), 8.87 (dd, 2H, CH, aryl), 8.52 (s, 1H, CH, aryl), 7.93 (q, 2H, aryl), 7.46 and 7.50 (m, 4H, CH, aryl).
6		7		88(95) [d]	Cyclopentanone (entry 6): 2.12 (t, 4H, COCH <sub>2</sub> ), 1.97 (m, 4H, CH <sub>2</sub> CH <sub>2</sub> );
7		5		92(97) [d]	Acetophenone (entry 7): 7.97 (d, 2H, aryl), 7.56 (t, 1H, aryl), 7.46 (t, 2H, aryl), 2.60 (s, 3H, COCH <sub>3</sub> );
8		6		94(98) [d]	4-Methylacetophenone 5 (entry 8): 7.54 (d, 2H, aryl), 6.6 (d, 2H, aryl), 2.65 (s, 3H, COCH <sub>3</sub> ); 2.55 (s, 3H, CH <sub>3</sub> );
9		8		91	<sup>1</sup> H Benzo[d]imidazole-2-carbaldehyde (entry 9): 9.82 (s, 1H, CHO), 7.62–7.22 (m, 4H, C <sub>6</sub> H <sub>4</sub> ), 4.9 (br s, 1H, NH);
10		8		90	1-(1H-Benzo[d]imidazol-2-yl)ethanone (entry 10): 10.1 (br s, 1H, NH), 7.90 (d, 1H, C <sub>6</sub> H <sub>4</sub> ), 7.5 (d, 1H, C <sub>6</sub> H <sub>4</sub> ), 7.41–7.35 (m, 2H, C <sub>6</sub> H <sub>4</sub> ), 2.8 (s, 3H, COCH <sub>3</sub> );

Table 3. Cont.

Entry	Substrate	Reaction Time	Product	Yield <sup>[b, c]</sup> (%)	<sup>1</sup> H NMR (300 MHz, CDCl <sub>3</sub> , δ ppm)
11		8		90	1-(1-Methylbenzo[d]imidazol-2-yl)ethanone (entry 11): 7.88 (d, 1H, C <sub>6</sub> H <sub>4</sub> ), 7.43 (d, 1H, C <sub>6</sub> H <sub>4</sub> ), 7.37 (m, 2H, C <sub>6</sub> H <sub>4</sub> ), 4.1 (s, 3H, NCH <sub>3</sub> ), 2.83 (s, 3H, COCH <sub>3</sub> );
12		9		89	1-(1-Benzoylbenzo[d]imidazol-2-yl)ethanone (entry 12): 8.08 (d, 1H, C <sub>6</sub> H <sub>4</sub> ), 7.69 (d, 1H, C <sub>6</sub> H <sub>4</sub> ), 7.63–7.60 (m, 2H, C <sub>6</sub> H <sub>4</sub> ), 7.49–7.42 (m, 5H, CO C <sub>6</sub> H <sub>4</sub> ), 2.72 (s, 3H, COCH C <sub>6</sub> H <sub>4</sub> );

<sup>[a]</sup> Oxidation reactions were performed at 1 atm O<sub>2</sub> using 1.0 mmol of substrate in 5 mL of toluene. <sup>[b]</sup> Isolated yields. <sup>[c]</sup> The compounds were determined by <sup>1</sup>H NMR analyses. <sup>[d]</sup> GC Conversion.

Next, we investigated the oxidation of secondary alcohols using CuO@GO. As can be seen, the oxidation of 1-phenyl ethanol and 1-(4-methyl phenyl) ethanol also underwent efficient oxidation to produce respective carbonyl compounds in high yields (92% and 94% (entries 7 and 8)). Next, we investigated the efficiency of CuO@GO for the oxidation of heterocyclic fused-ring aromatic alcohols. For example, the oxidation of (1H-benzo[d]imidazole-2-yl) methanol was converted into its oxidized product of (1H-benzo[d]imidazole-2-yl)methanone in a good yield (~91%) (entry 9). Interestingly, CuO@GO is also highly dynamic for the oxidation of 2-hydroxyethyl benzimidazole [24–37], and its n-methyl analogs produce their carbonyl counterpart in high yields (~90%) (entries 10 and 11). Furthermore, the oxidation was strongly affected by the steric bulkiness of the N-phenyl methanone-2-hydroxy ethyl benzimidazole to the corresponding ketone in good yield (89%) (entry 12) [24,29,40–45]. Using CuO@GO as a catalyst, higher yields were obtained from N-substituted benzimidazole into corresponding ketones over conventional methods [46–53]. It was apparent that the catalyst CuO@GO can accelerate oxidation reaction in high yields.

### 3. Experimental Section

#### 3.1. Materials, Methods, and Characterization

All the reagents are analytical grade and were used without further purification. High-purity natural graphite (99%, average size 200 μm) was purchased from Infracore, Seoul, Korea. The copper (II) acetate, sodium nitrate, sulfuric acid, hydrogen peroxide, and all the reagents at analytical grade were procured from Aldrich Chemical Co., St. Louis, MO, USA, and used without further purification. The numerous functional groups present on the CuO-NPs, GO, and CuO@GO were measured using a Nicolet 6700 FT-IR spectrophotometer, Madison, WI USA. Diffraction data was acquired by a Rigaku high-power X-ray, diffractometer, Wilmington, MA, USA. TEM measurement is executed using JEOL, high-resolution transmission electron microscope (HRTEM) by spurt voltage of 200 kV, Pleasanton, CA, USA; specimens were arranged by depositing a drop of trial dispersion on 300 mesh carbon-coated Cu grids. Specimen morphologies were determined using Hitachi cold FE-SEM at 10 kV, Tokyo, Japan. XPS analysis was performed on a K-alpha analyzer (Thermo Fisher Scientific, Waltham MA, USA). Melting points were measured on an electrothermal 9100 apparatus. The contents of Cu in the synthesized CuO@GO were determined using Leeman Prodigy Spec inductively coupled plasma atomic emission spectroscopy (ICP-AES, Leicestershire, UK) and an elemental analyzer (Vario EL III, Vienna, Austria). To measure the CuO@GO weight loss, the samples were placed and heated at a rate of 10/min from 30 °C to 700 °C, and Cu ions were analyzed by ICP-AES. Products were characterized by comparison with authentic samples, and spectroscopic

data.  $^1\text{H}$ NMR spectra were recorded on a Bruker 300 MHz spectrophotometer, (San Jose, CA, USA) in  $\text{CDCl}_3$  using TMS as an internal standard.

### 3.2. Synthesis of Graphene Oxide (GO)

GO was prepared from natural graphite using the well-known Hummer method with minor alterations. In a dry 250 mL of 3 neck beaker, 2.0 g of natural graphite was added, followed by 1.0 g  $\text{NaNO}_3$  and 46 mL of  $\text{H}_2\text{SO}_4$ , while stirring in an ice bath. Subsequently, 6.0 g of  $\text{KMnO}_4$  were gradually added to the beaker while stirring at 20 °C. After 4 min, the ice bath was removed, then the reaction mixture was maintained at 35 °C for half an hour, and subsequently 92 mL of DI water was added slowly to the reaction pot, and then stirred for another 15 min. Subsequently, 80 mL of hot water and 20 mL of 30%  $\text{H}_2\text{O}_2$  at 60 °C were added to reduce the residual  $\text{KMnO}_4$ , and the product was stirred till no bubbles appeared. To end, the reaction mixture was centrifuged at 10,000 rpm for about 30 min. The supernatant was discarded and obtained. The wet cake was washed with warm water until the pH was ~7. The acquired yellow-brown slurry cake was re-dispersed in DI water, and bath-sonicated for 30 min. The GO powder was collected after drying the suspensions at 60 °C.

### 3.3. Synthesis of CuO-NPs

In this procedure, a solution of  $\text{Cu}(\text{OAc})_2 \cdot 2\text{H}_2\text{O}$  (20 mL, 0.25 M) was made into alkaline by the addition of ammonium hydroxide ( $\text{NH}_4\text{OH}$ ), subsequently, the reaction mixture was converted into a deep-blue color. Next, a solution of SLS in ethylene glycol (EG) (10 mL, 0.01 M) was added and agitated for 15 min. Next, glucose (2.5 g) was added and heated to 75 °C while stirring. When the color of the solution changed from blue to golden yellow, 5 vol% of sulfuric acid was added to neutralize the reaction mixture. Lastly, the brown solution was cooled to attain a cuprous oxide nanoparticles fluid; the supernatant liquid was decanted after centrifugation at 8000 rpm to acquire solid CuO nanoparticles (CuO NPs).

### 3.4. Synthesis of CuO@GO

Nanocomposites with different mass ratios of CuO@GO were synthesized. The mass of CuO was determined by the  $\text{Cu}(\text{OAc})_2$  rendering to the hydrolysis reaction. Allowing for the yield percentage of CuO in the authentic procedure,  $\text{Cu}(\text{OAc})_2 \cdot \text{H}_2\text{O}$  was reserved in considerable excess. In the typical route, 0.05 g of dried GO was suspended in 50 mL of isopropanol and sonicated for 30 min to give a brown dispersion. The resulting homogeneous dispersion was mixed with 0.07 g of  $\text{Cu}(\text{OAc})_2 \cdot \text{H}_2\text{O}$  in a three-neck RBF, and equipped with a reflux condenser. The mixture was heated to approximately 82 °C with vigorous stirring and maintained for 2 h. Then, 5 mL of DI water was quickly introduced into the reaction pot, and the mixture has been heated at 83 °C for an additional 30 min. During this procedure, the deep-brown colored dispersion was slowly turned into a black color. Afterward, the reaction pot was allowed to room temperature. The as-synthesized CuO@GO nanocomposites were centrifuged, washed with fresh ethanol several times until removed from occluded water, and dried at 60 °C in a hot-air oven overnight.

### 3.5. General Oxidation Protocol

In the typical oxidation reaction, the CuO@GO (70 mg, 2 mol %) was re-dispersed in 10 mL of toluene assisted by ultra-sonication, followed by the addition of starting alcohol (1 mmol) and anisole (0.1 mmol). Superior dispersions were obtained for the CuO@GO as compared to GO due to strong intercalation of GO nano sheets by invasion of CuO NPs. The tube holding the reaction mixture was associated with a reaction station which was provided by stirring and heating at 80 °C for 6h. The reaction was carried out under 1 atm of the  $\text{O}_2$  balloon as the oxidant. After the disappearance of starting material, methylene chloride (15 mL) was added to the flask, and the reaction mixture remained filtered using a sintered glass funnel. The residue was gently washed with extra-methylene chloride

(2 × 10 mL), followed by saturated NaCl solution (50 mL), and dried over anhydrous MgSO<sub>4</sub> and solvent were evaporated on a rotary evaporator. The crude product was purified by column chromatography using a mixture of ethyl acetate and n-hexane (1:4 v/v) as an eluent. All the products were analyzed using <sup>1</sup>H NMR spectroscopy.

### 3.6. ICP-AES Analysis

The CuO@GO was dissolved in a suitable solvent and used for ICP-AES analysis. It is similar to XRF sample preparation, and was developed to avoid dealing with hydrofluoric acid in the shipboard environment. A dried CuO@GO was powdered by crushing the sample between two plastic disks in a hydraulic press. Powder was produced by grinding pieces <1 cm in diameter in a Spex Shatterbox 8530, using a tungsten carbide grinding vessel. Characteristically, 0.1 g of CuO@GO was mixed with 0.4 g ultrapure-grade LiBO<sub>2</sub> flux and LiBr wetting agent in a Pt-Au crucible. This mixture was fused at 1050 °C for 10–12 min. After the bead cooled, and it was dissolved in HNO<sub>3</sub>. A small amount of filtered solution was diluted by additional HNO<sub>3</sub>. This method was superior and gave good results in a stable sample solution.

## 4. Conclusions

In conclusion, we have established an easy and highly efficient method for the oxidation of alcohols into carbonyl compounds in good-to-excellent yields using a recyclable CuO@GO heterogeneous catalyst. Mainly, Cu atoms are anchored to the oxygen functional groups of GO, such as –OH, COOH, and CO. We found this catalyst to be highly active and stable even in an O<sub>2</sub>-rich reaction atmosphere under variable load conditions and temperatures up to 80 °C. In addition, it is highly selective (98%) for the oxidation of alcohols into ketones in the presence of up to 90% O<sub>2</sub> in the gas feed. After completion of the reaction, the catalyst was separated easily by centrifugation followed by filtration for reusability. Then it was reused in four consecutive cycles. The leaching experiments evidenced that the catalyst activity remains strong until the fourth re-use cycle, due to the strong dispersibility of the catalyst. In addition, TOF showed superiority compared to CuO NPs-based catalysts. The green chemistry protocol can strongly eradicate the use of hazardous solvents, expensive catalysts, and long reaction times. In addition, it can reduce the experimental cost and be commercially viable to bulk production. This method should be applicable for the oxidation of aromatic, aliphatic, and benzimidazolyl alcohols into their corresponding carbonyl compounds in high yields. Mainly, the oxidation state of Cu metal in the active catalyst is as Cu<sup>+2</sup> and it can be strongly chelated with the host GO nanosheets. Currently, our team is optimizing and expanding the scope of this oxidation process and investigating its applications in other organic transformations.

**Author Contributions:** Conceptualization, M.A.M., R.S., N.A. and R.K.C.; data curation, M.A.M., R.S., N.A., R.K.C., A.A.A. and K.A.A.; formal analysis, R.S., N.A. and R.K.C.; investigation, M.A.M., R.S., N.A. and R.K.C.; methodology, R.S., N.A. and R.K.C.; project administration, M.A.M., Software, A.A.A. and K.A.A.; supervision, M.A.M., R.S., N.A. and R.K.C.; validation, R.S., N.A. and R.K.C.; writing—original draft, M.A.M., R.S., N.A. and R.K.C.; writing—review and editing, R.S., N.A., R.K.C., A.A.A. and K.A.A. All authors have read and agreed to the published version of the manuscript.

**Funding:** Institutional Fund Projects under grant number (IFPIP: 1406-130-1442) by the Ministry of Education and King Abdulaziz University, DSR, Jeddah, Saudi Arabia.

**Data Availability Statement:** All data created is provided in this manuscript.

**Acknowledgments:** This research work was funded by the Institutional Fund Projects under grant number (IFPIP: 1406-130-1442). Therefore, authors gratefully acknowledge technical and financial support from the Ministry of Education and King Abdulaziz University, DSR, Jeddah, Saudi Arabia.

**Conflicts of Interest:** The authors declare no conflict of interest.

## References

1. Stahl, S.S. Palladium-catalyzed oxidation of organic chemicals with O<sub>2</sub>. *Science* **2005**, *309*, 1824–1826. [[CrossRef](#)] [[PubMed](#)]
2. Ohtaka, A.; Kono, Y.; Inui, S.; Yamamoto, S.; Ushiyama, T.; Shimomura, O.; Nomura, R. Linear polystyrene-stabilized Pt nanoparticles for aerobic alcohol oxidation and hydrogen-transfer reduction in aqueous media. *J. Mol. Catal. A Chem.* **2012**, *360*, 48–53. [[CrossRef](#)]
3. Schrunner, M.; Proch, S.; Mei, Y.; Kempe, R.; Miyajima, N.; Ballauff, M. Stable bimetallic gold–platinum nanoparticles immobilized on spherical polyelectrolyte brushes: Synthesis, characterization, and application for the oxidation of alcohols. *Adv. Mater.* **2008**, *20*, 1928–1933. [[CrossRef](#)]
4. Hong, Y.; Yan, X.; Liao, X.; Li, R.; Xu, S.; Xiao, L.; Fan, J. Platinum nanoparticles supported on Ca (Mg)-zeolites for efficient room-temperature alcohol oxidation under aqueous conditions. *Chem. Commun.* **2014**, *50*, 9679–9682. [[CrossRef](#)]
5. Tojo, G.; Fernández, M. Oxidation of primary alcohols to carboxylic acids. In *A Guide to Current Common Practice*; Springer: Santiago de Compostela, Spain, 2007; Volume 132.
6. Ali, R.; Adil, S.; Al-warthan, A.; Siddiqui, M.R.H. Identification of active phase for selective oxidation of benzyl alcohol with molecular oxygen catalyzed by copper-manganese oxide nanoparticles. *J. Chem.* **2013**, *2013*, 367261. [[CrossRef](#)]
7. Tojo, G.; Fernández, M. Ruthenium tetroxide and other ruthenium compounds. In *Oxidation of Primary Alcohols to Carboxylic Acids*; Springer: Santiago de Compostela, Spain, 2007; pp. 61–78.
8. Wang, H.; Fan, W.; He, Y.; Wang, J.; Kondo, J.N.; Tatsumi, T. Selective oxidation of alcohols to aldehydes/ketones over copper oxide-supported gold catalysts. *J. Catal.* **2013**, *299*, 10–19. [[CrossRef](#)]
9. Poreddy, R.; Engelbrekt, C.; Riisager, A. Copper oxide as efficient catalyst for oxidative dehydrogenation of alcohols with air. *Catal. Sci. Technol.* **2015**, *5*, 2467–2477. [[CrossRef](#)]
10. Mallat, T.; Baiker, A. Oxidation of alcohols with molecular oxygen on solid catalysts. *Chem. Rev.* **2004**, *104*, 3037–3058. [[CrossRef](#)]
11. Namboodiri, V.V.; Polshettiwar, V.; Varma, R.S. Expedient oxidation of alcohols to carbonyl compounds using iron (III) nitrate. *Tetrahedron Lett.* **2007**, *48*, 8839–8842. [[CrossRef](#)]
12. Jerome, P.; Kausalya, G.; Thangadurai, T.D.; Karvembu, R. Green synthesis of CuO nanoflakes from copper pincer complex for effective N-arylation of benzimidazole. *Catal. Commun.* **2016**, *75*, 50–54. [[CrossRef](#)]
13. da Silva Neto, E.H.; Comin, R.; He, F.; Sutarto, R.; Jiang, Y.; Greene, R.L.; Sawatzky, G.A.; Damascelli, A. Charge ordering in the electron-doped superconductor Nd<sub>2-x</sub>Ce<sub>x</sub>CuO<sub>4</sub>. *Science* **2015**, *347*, 282–285. [[CrossRef](#)]
14. Zhang, P.-P.; Zhang, H.; Sun, X.-H. A uniform porous multilayer-junction thin film for enhanced gas-sensing performance. *Nanoscale* **2016**, *8*, 1430–1436. [[CrossRef](#)] [[PubMed](#)]
15. Zhang, H.; Zhang, G.; Li, Z.; Qu, K.; Wang, L.; Zeng, W.; Zhang, Q.; Duan, H. Ultra-uniform CuO/Cu in nitrogen-doped carbon nanofibers as a stable anode for Li-ion batteries. *J. Mater. Chem. A* **2016**, *4*, 10585–10592. [[CrossRef](#)]
16. Wang, G.; Huang, B.; Wang, L.; Wang, Z.; Lou, Z.; Qin, X.; Zhang, X.; Dai, Y. CuO/CuSCN valence state heterojunctions with visible light enhanced and ultraviolet light restrained photocatalytic activity. *Chem. Commun.* **2014**, *50*, 3814–3816. [[CrossRef](#)]
17. Xia, Y.; Pu, X.; Liu, J.; Liang, J.; Liu, P.; Li, X.; Yu, X. CuO nanoleaves enhance the c-Si solar cell efficiency. *J. Mater. Chem. A* **2014**, *2*, 6796–6800. [[CrossRef](#)]
18. Li, F.; Li, J.-F.; Li, J.-H.; Yao, F.-Z. The effect of Cu substitution on microstructure and thermoelectric properties of LaCoO<sub>3</sub> ceramics. *Phys. Chem. Chem. Phys.* **2012**, *14*, 12213–12220. [[PubMed](#)]
19. Cui, P.; Wang, A.-J. Synthesis of CNTs/CuO and its catalytic performance on the thermal decomposition of ammonium perchlorate. *J. Saudi Chem. Soc.* **2016**, *20*, 343–348. [[CrossRef](#)]
20. Lee, C.; Wei, X.; Kysar, J.W.; Hone, J. Measurement of the elastic properties and intrinsic strength of monolayer graphene. *Science* **2008**, *321*, 385–388.
21. Bunch, J.S.; Verbridge, S.S.; Alden, J.S.; Van Der Zande, A.M.; Parpia, J.M.; Craighead, H.G.; McEuen, P.L. Impermeable atomic membranes from graphene sheets. *Nano Lett.* **2008**, *8*, 2458–2462.
22. Loh, K.P.; Bao, Q.; Eda, G.; Chhowalla, M. Graphene oxide as a chemically tunable platform for optical applications. *Nat. Chem.* **2010**, *2*, 1015–1024. [[CrossRef](#)]
23. Meric, I.; Han, M.Y.; Young, A.F.; Ozyilmaz, B.; Kim, P.; Shepard, K.L. Current saturation in zero-bandgap, top-gated graphene field-effect transistors. *Nat. Nanotechnol.* **2008**, *3*, 654–659. [[CrossRef](#)] [[PubMed](#)]
24. Kwon, M.S.; Kim, N.; Seo, S.H.; Park, I.S.; Cheedra, R.K.; Park, J. Recyclable palladium catalyst for highly selective  $\alpha$  alkylation of ketones with alcohols. *Angew. Chem. Int. Ed.* **2005**, *44*, 6913–6915. [[CrossRef](#)] [[PubMed](#)]
25. Kwon, M.S.; Kim, S.; Park, S.; Bosco, W.; Chidra, R.K.; Park, J. One-pot synthesis of imines and secondary amines by Pd-catalyzed coupling of benzyl alcohols and primary amines. *J. Org. Chem.* **2009**, *74*, 2877–2879. [[CrossRef](#)] [[PubMed](#)]
26. Chen, J.; Yao, B.; Li, C.; Shi, G. An improved Hummers method for eco-friendly synthesis of graphene oxide. *Carbon* **2013**, *64*, 225–229. [[CrossRef](#)]
27. Marcano, D.C.; Kosynkin, D.V.; Berlin, J.M.; Sinitskii, A.; Sun, Z.; Slesarev, A.; Alemany, L.B.; Lu, W.; Tour, J.M. Improved synthesis of graphene oxide. *ACS Nano* **2010**, *4*, 4806–4814. [[CrossRef](#)]
28. Wu, Z.-S.; Yang, S.; Sun, Y.; Parvez, K.; Feng, X.; Müllen, K. 3D nitrogen-doped graphene aerogel-supported Fe<sub>3</sub>O<sub>4</sub> nanoparticles as efficient electrocatalysts for the oxygen reduction reaction. *J. Am. Chem. Soc.* **2012**, *134*, 9082–9085. [[CrossRef](#)]
29. Cheedarala, R.K.; Park, E.J.; Park, Y.B.; Park, H.W. Highly wettable CuO: Graphene oxide core-shell porous nanocomposites for enhanced critical heat flux. *Phys. Status Solidi A* **2015**, *212*, 1756–1766. [[CrossRef](#)]

30. Zhang, S.; Gao, W.; Li, J.; Zhou, X.; Qu, Y. Interfacial effects of the CuO/GO composite to mediate the side reactions of N, N-dimethylformamide fragments. *ACS Appl. Mater. Interfaces* **2014**, *6*, 22174–22182. [[CrossRef](#)]
31. Vaseem, M.; Umar, A.; Kim, S.H.; Hahn, Y.-B. Low-temperature synthesis of flower-shaped CuO nanostructures by solution process: Formation mechanism and structural properties. *J. Phys. Chem. C* **2008**, *112*, 5729–5735. [[CrossRef](#)]
32. Taratayko, A.; Kolobova, E.; Mamontov, G. Graphene Oxide Decorated with Ag and CeO<sub>2</sub> Nanoparticles as a Catalyst for Room-Temperature 4-Nitrophenol Reduction. *Catalysts* **2022**, *12*, 1393. [[CrossRef](#)]
33. Yang, Z.; Sun, S.; Kong, C.; Song, X.; Ding, B. Designated-tailoring on {100} facets of Cu<sub>2</sub>O nanostructures: From octahedral to its different truncated forms. *J. Nanomater.* **2010**, *2010*, 710584. [[CrossRef](#)]
34. Karthikeyan, N.; Philip, J.; Raj, B. Effect of clustering on the thermal conductivity of nanofluids. *Mater. Chem. Phys.* **2008**, *109*, 50–55. [[CrossRef](#)]
35. Poulston, S.; Parlett, P.; Stone, P.; Bowker, M. Surface oxidation and reduction of CuO and Cu<sub>2</sub>O studied using XPS and XAES. *Surf. Interface Anal.* **1996**, *24*, 811–820. [[CrossRef](#)]
36. Abad, A.; Corma, A.; García, H. Catalyst parameters determining activity and selectivity of supported gold nanoparticles for the aerobic oxidation of alcohols: The molecular reaction mechanism. *Chem. A Eur. J.* **2008**, *14*, 212–222. [[CrossRef](#)] [[PubMed](#)]
37. Gopiraman, M.; Deng, D.; Ganesh Babu, S.; Hayashi, T.; Karvembu, R.; Kim, I.S. Sustainable and versatile CuO/GNS nanocatalyst for highly efficient base free coupling reactions. *ACS Sustain. Chem. Eng.* **2015**, *3*, 2478–2488. [[CrossRef](#)]
38. Kwon, M.S.; Kim, N.; Park, C.M.; Lee, J.S.; Kang, K.Y.; Park, J. Palladium nanoparticles entrapped in aluminum hydroxide: Dual catalyst for alkene hydrogenation and aerobic alcohol oxidation. *Org. Lett.* **2005**, *7*, 1077–1079. [[CrossRef](#)] [[PubMed](#)]
39. Sharma, M.; Das, B.; Sharma, M.; Deka, B.K.; Park, Y.B.; Bhargava, S.K.; Usum, K.; Bania, K.K. Pd/Cu-Oxide Nanoconjugate at Zeolite-Y Crystallite Crafting the Mesoporous Channels for Selective Oxidation of Benzyl-Alcohols. *ACS Appl. Mater. Interfaces* **2017**, *9*, 35453–35462. [[CrossRef](#)]
40. Cheedarala, R.K.; Park, E.; Kong, K.; Park, Y.-B.; Park, H.W. Experimental study on critical heat flux of highly efficient soft hydrophilic CuO–chitosan nanofluid templates. *Int. J. Heat Mass Transf.* **2016**, *100*, 396–406. [[CrossRef](#)]
41. Cheedarala, R.K.; Song, J.I. In situ generated hydrophobic micro ripples via  $\pi$ - $\pi$  stacked pop-up reduced graphene oxide nanoflakes for extended critical heat flux and thermal conductivities. *RSC Adv.* **2019**, *9*, 31735–31746. [[CrossRef](#)]
42. Dandia, A.; Bansal, S.; Sharma, R.; Rathore, K.; Parewa, V. Microwave-assisted nanocatalysis: A CuO NPs/rGO composite as an efficient and recyclable catalyst for the Petasis-borono–Mannich reaction. *RSC Adv.* **2018**, *8*, 30280–30288. [[CrossRef](#)]
43. Torbina, V.V.; Vodyankin, A.A.; Ten, S.; Mamontov, G.V.; Salaev, M.A.; Sobolev, V.I.; Vodyankina, O.V. Ag-Based Catalysts in Heterogeneous Selective Oxidation of Alcohols: A Review. *Catalysts* **2018**, *8*, 447. [[CrossRef](#)]
44. Cheedarala, R.K.; Sunkara, V.; Park, J.W. Facile synthesis of second-generation dendrons with an orthogonal functional group at the focal point. *Synth. Commun.* **2009**, *39*, 1966–1980. [[CrossRef](#)]
45. Cheedra, R.K.; Sachwani, R.; Krishna, P.R. Lipase mediated kinetic resolution of benzimidazolyl ethanols. *Tetrahedron Asymmetry* **2008**, *19*, 901–905. [[CrossRef](#)]
46. Jeon, J.H.; Cheedarala, R.K.; Kee, C.D.; Oh, I.K. Dry-type artificial muscles based on pendent sulfonated chitosan and functionalized graphene oxide for greatly enhanced ionic interactions and mechanical stiffness. *Adv. Funct. Mater.* **2013**, *23*, 6007–6018. [[CrossRef](#)]
47. Rao, T.N.; AlOmar, S.Y.; Ahmed, F.; Albalawi, F.; Ahmad, N.; Rao, N.K.; Rao, M.B.; Cheedarala, R.K.; Reddy, G.R.; Naidu, T.M. Reusable nano-zirconia-catalyzed synthesis of benzimidazoles and their antibacterial and antifungal activities. *Molecules* **2021**, *26*, 4219. [[CrossRef](#)]
48. Cheedarala, R.K.; Chidambaram, R.R.; Siva, A.; Song, J.I. An aerobic oxidation of alcohols into carbonyl synthons using bipyridyl-cinchona based palladium catalyst. *RSC Adv.* **2021**, *11*, 32942–32954. [[CrossRef](#)]
49. Gaikwad, S.; Cheedarala, R.K.; Gaikwad, R.; Kim, S.; Han, S. Controllable Synthesis of 1, 3, 5-tris (1H-benzo [d] imidazole-2-yl) Benzene-Based MOFs. *Appl. Sci.* **2021**, *11*, 9856. [[CrossRef](#)]
50. Kassem, A.A.; Abdelhamid, H.N.; Fouad, D.M.; Ibrahim, S.A. Catalytic reduction of 4-nitrophenol using copper terephthalate frameworks and CuO@C composite. *J. Environ. Chem. Eng.* **2021**, *9*, 104401. [[CrossRef](#)]
51. Kassem, A.A.; Abdelhamid, H.N.; Fouad, D.M.; Ibrahim, S.A. Metal-organic frameworks (MOFs) and MOFs-derived CuO@C for hydrogen generation from sodium borohydride. *Int. J. Hydrogen Energy* **2019**, *44*, 31230–31238. [[CrossRef](#)]
52. Chidambaram, R.; Ramaswamy, R.R.; Koppurapu, I.; Raykar, A.; Kulkarani, A.; Vijaya Sankar, A.V.; Siva Ayyanar, S.; Nagarjuna, A.; Cheedarala, R.K. A continuous protocol for the epoxidation of olefins, monocyclic terpenes, and Alpha Beta Unsaturated Carbonyl Synthons using eco-friendly Flow Reactor Conditions. *Results Eng.* **2022**, *16*, 100652.
53. Dhinakaran, G.; Harichandran, G.; Suvaitha, S.P.; Venkatachalam, K. Catalytic activity of SBA-15 supported CuO for selective oxidation of veratryl alcohol to veratraldehyde. *Mol. Catal.* **2022**, *528*, 112454. [[CrossRef](#)]

**Disclaimer/Publisher’s Note:** The statements, opinions and data contained in all publications are solely those of the individual author(s) and contributor(s) and not of MDPI and/or the editor(s). MDPI and/or the editor(s) disclaim responsibility for any injury to people or property resulting from any ideas, methods, instructions or products referred to in the content.